

An iterative method for solving the dynamic response of railway vehicle-track coupled systems based on prediction of wheel-rail forces



Wei Wang^a, Yahui Zhang^{a,*}, Huajiang Ouyang^{a,b}

^a State Key Laboratory of Structural Analysis for Industrial Equipment, Department of Engineering Mechanics, International Center for Computational Mechanics, Dalian University of Technology, Dalian 116023, PR China

^b School of Engineering, University of Liverpool, The Quadrangle, Liverpool L69 3GH, UK

ARTICLE INFO

Article history:

Received 25 April 2017

Revised 25 July 2017

Accepted 11 August 2017

Keywords:

Vehicle-track dynamic interaction

Iterative method

Weighted least-squares error predictor

Wheel-rail contact relation

Track irregularity

ABSTRACT

An iterative method based on prediction of wheel-rail forces is presented to determine the dynamic response of railway vehicle-track coupled systems. The key idea of the present method lies in the modification of the starting value of each step during the iteration by prediction. The conventional iterative method begins iteration of the current step at the previously converged value of the wheel-rail forces. However, in the present method, the predicted wheel-rail forces by the Weighted Least-Squares Error (WLSE) predictor are used as the starting value for the current step. The equations of motion of the vehicle and the track subsystems are established separately and solved iteratively. According to the response of the wheelsets and the rails, and considering the track irregularity, the predicted wheel-rail forces are corrected by the wheel-rail interaction model in which detailed wheel rail contact geometry relations and nonlinear wheel rail creep forces are taken into account. The relaxation technique is adopted to solve the problem of numerical diffusion in the iterative process.

A moving vehicle travelling on a two layer flexible track is considered in this study. The accuracy of the proposed method is verified by comparing the results obtained from the present method with the results from the commercial software NUCARS and the efficiency are verified by comparing with the conventional iterative method. Numerical results show that the present method not only gives results comparable to those using the NUCARS software in terms of accuracy, but also saves at least 25% computational cost compared with the conventional iterative method. With the nonlinear wheel-rail contact relation fully considered, the present method can get more detailed results of the vehicle-track coupled model. Meanwhile, the efficiency of the present method is enhanced by means of prediction of wheel-rail forces with the WLSE predictor.

© 2017 Elsevier Ltd. All rights reserved.

1. Introduction

The dynamic model of the vehicle-track coupled system and its solution method are essential to a series of advanced studies, such as evaluation of running safety and ride comfort performance of high speed trains, prediction of wheel wear and vibration noise. The numerical results can be used as a theoretic guidance for finding out the cause of some practical engineering problems such as out of round wheels, rail corrugation, identifying the sources of vibration or noise, and developing solutions or treatments to those problems. Therefore, it is of significance to solve the dynamic response of the vehicle-track coupled system efficiently and accurately.

The dynamic response of the vehicle-track coupled system can be solved in either the frequency or the time domain [1]. The frequency method is applicable for efficient solution of infinite length or periodic track structures, especially for the solution of wheel-rail dynamic interaction at high frequencies, but the time domain solution appears to be necessary where there are significant nonlinearities such as wheel rail contact geometry relation and stick-slip.

For solving the dynamic response of the vehicle and track system in time domain, there are mainly two methods available: the coupled method and the iterative method. The coupled method considers the vehicle and the track subsystems as a whole and solves the coupled system equations without any iteration by a step-by-step integration method. However, the system coefficient matrices vary according to the position of the vehicles on the track and must be updated and decomposed at every time step. This will reduce the computational efficiency. Another drawback is that the

* Corresponding author.

E-mail address: zhangyh@dlut.edu.cn (Y. Zhang).

formulation of coefficient matrices depend on both the vehicle and track models, that is to say, all coefficients must be changed if a new type of vehicle or track is introduced. The iterative method can effectively avoid these shortcomings.

In the iterative method, the whole system is divided into two subsystems at the interface of vehicle and track. The two subsystems are coupled by enforcing equilibrium of forces and compatibility of displacements at the contact points between the wheels and the rails. The equations of motion of the two subsystems are solved separately with an iterative procedure. Green and Cebon [2,3] involved convolution of the vehicle loads with modal response of the bridge to predict its dynamic response under a given set of vehicle wheel loads and extended this method to include dynamic interaction between the vehicle and bridge by an iterative procedure. Yang and Fonder [4] presented an iterative method to solve the dynamic response of the Yangtze-River Bridge at Wuhan under a moving train with 2 locomotives and 4 freight vehicles. Xu et al. [5] performed dynamic analysis of coupled train and cable-stayed bridge systems in cross winds with an iterative procedure. Majka and Hartnett [6] developed a numerical model which incorporated a three dimensional multi-body train and a finite element bridge to investigate the effects of various parameters, such as the speed of the train, train-to-bridge frequency, mass and span ratios, bridge damping, on the dynamic response of railway bridges with a modified Newton-Raphson iterative procedure. Zhang et al. [7] proposed a coupled wind-vehicle-bridge dynamic model which considered the shielding effect of bridge tower with triangular wind barriers and solved the vehicle-bridge dynamic equations with time-varying external loads. Nguyen et al. [8] considered the vehicles and substructure as two separate systems interacting through a proposed wheel-rail contact model and proposed a new iterative scheme for solution of wheel-rail contact forces and checking contact loss. Hawk and Ghali [9] proposed an analytical procedure called the iterative dynamic substructuring method (IDSM) to solve the response of a beam-slab bridge system traversed by multi-axle trucks without consideration of roughness effects. Marchesiello et al. [10] dealt with the interaction of a multi-span continuous bridges modelled by isotropic plates with a vehicle modelled by seven degrees of freedom mass-spring-damper system moving at constant speed and computed the dynamic response of the vehicle and the bridge iteratively. Feriani et al. [11] studied the dynamic interaction between a travelling vehicle and a bridge and compared both the performance and the efficiency of the two iterative procedures which performed either on the whole time history (WTH) or in the single time step (STS). Vincenzi et al. [12] analyzed the dynamic interaction between trains and a bridge and carried out a parametric investigation, including the influence of the travelling speed and the weight of the train on dynamic response. Lei et al. [13] presented a cross iteration algorithm to solve the dynamic response of the China's high speed train CRH3 vehicle and slab track coupling system. Li et al. [14] developed a computer-aided numerical method for analyzing coupled railway vehicle-bridge systems of nonlinear features and investigated the convergence of iterative computation schemes with and without wheel jumps. In the iterative method, the decomposition of the coefficient matrices at every time step can be avoided and thus a more efficient solution method can be developed separately according to the structural characteristics of each subsystem. But it is worth noting that the iteration process may not be easy to converge or converge slowly, especially for large-scale structures. These disadvantages restrict the scope of application of the iterative method.

To overcome the drawbacks of the aforementioned solution methods, an iterative solution method based on prediction of wheel rail forces is proposed and verified in this paper. The wheel-rail forces are predicted by the WLSE predictor and then

substituted into the equations of motion of the vehicle and track separately to solve the dynamic response of each subsystem. According to the response of the wheelsets and the rails, considering the track irregularity, the predicted contact forces are corrected by the wheel-rail interaction model. If the difference between the corrected and the predicted forces is greater than the specified tolerance, iteration continues until convergence is achieved. The relaxation technique is adopted to avoid the problem of numerical diffusion in the iterative process. Taking the CRH2 vehicle [15] running on a straight track as an example, the dynamic response of the vehicle to different types of track irregularities is solved in time domain by the present method, the conventional iterative method and NUCARS, respectively. The accuracy of the present method is demonstrated through a detailed comparison of numerical results with NUCARS and the efficiency is verified by comparing the computation cost with the conventional iterative method.

2. Vehicle-track coupled dynamic model

The iterative method proposed in this paper is not limited to the types of vehicles and track. Due to the limitation of the modelling capabilities of the track structure in NUCARS, the track is modelled as two parallel Euler beams with a finite length laid on two-layer flexible point supports. The vehicle is modelled as a mass-spring-damper system with 35 DOFs. The predicted wheel-rail forces are corrected by the wheel-rail interaction model to consider the nonlinear effects related to wheel-rail contact.

2.1. Equations of motion of vehicle subsystem

The CRH2 is one of the high-speed trains running in China, with the operating speed of 200 km per hour. Based on the structural characteristics of the CRH2 vehicle, a three dimensional dynamic model for one single vehicle is developed in this paper, composed by one car body resting on two frames and four wheelsets, as shown in Fig. 1. The car body, frames and wheelsets are all modelled as rigid bodies. Each rigid body is assigned with 5 DOFs, which are the lateral y , vertical z , roll ϕ , pitch β and yaw ψ , while the longitudinal motion is supposed to be known and characterized by a constant speed V . Thus the total number of DOFs of the vehicle model is 35. For convenience, the front and rear frames are numbered 1 and 2 respectively; the wheelset at the front of the vehicle along the running direction is numbered 1 and others are numbered 2, 3 and 4 consecutively. The left wheels or rail refer to the wheels or rail on the left when viewed from the front. Such a 35-DOF model is widely used, for example, in [16,17].

By assuming motion about the static equilibrium position, the equations of motion of the vehicle can be written as

$$\mathbf{M}_v \ddot{\mathbf{X}}_v + \mathbf{C}_v \dot{\mathbf{X}}_v + \mathbf{K}_v \mathbf{X}_v = \mathbf{F}_{vt} \quad (1)$$

where \mathbf{X}_v , $\dot{\mathbf{X}}_v$ and $\ddot{\mathbf{X}}_v$ are the vectors of displacement, velocity and acceleration of the vehicle subsystem, respectively. The displacement vector \mathbf{X}_v can be written as

$$\mathbf{X}_v = \left\{ \mathbf{x}_c^T, \mathbf{x}_{t_1}^T, \mathbf{x}_{t_2}^T, \mathbf{x}_{w_1}^T, \mathbf{x}_{w_2}^T, \mathbf{x}_{w_3}^T, \mathbf{x}_{w_4}^T \right\}^T \quad (2)$$

Subscripts “c”, “ t_1 ”, “ t_2 ”, “ w_1 ”, “ w_2 ”, “ w_3 ” and “ w_4 ” denote the car body, front frame, rear frame and wheelsets 1–4 respectively.

$$\mathbf{x}_i = \{y_i, z_i, \phi_i, \beta_i, \psi_i\}^T, \quad i = c, t_1, t_2, w_1, w_2, w_3, w_4 \quad (3)$$

\mathbf{M}_v , \mathbf{K}_v , \mathbf{C}_v are the mass, stiffness and damping matrices of the vehicle system respectively and can be expressed as follows

$$\mathbf{M}_v = \text{diag}[\mathbf{M}_c, \mathbf{M}_{t_1}, \mathbf{M}_{t_2}, \mathbf{M}_{w_1}, \mathbf{M}_{w_2}, \mathbf{M}_{w_3}, \mathbf{M}_{w_4}] \quad (4)$$

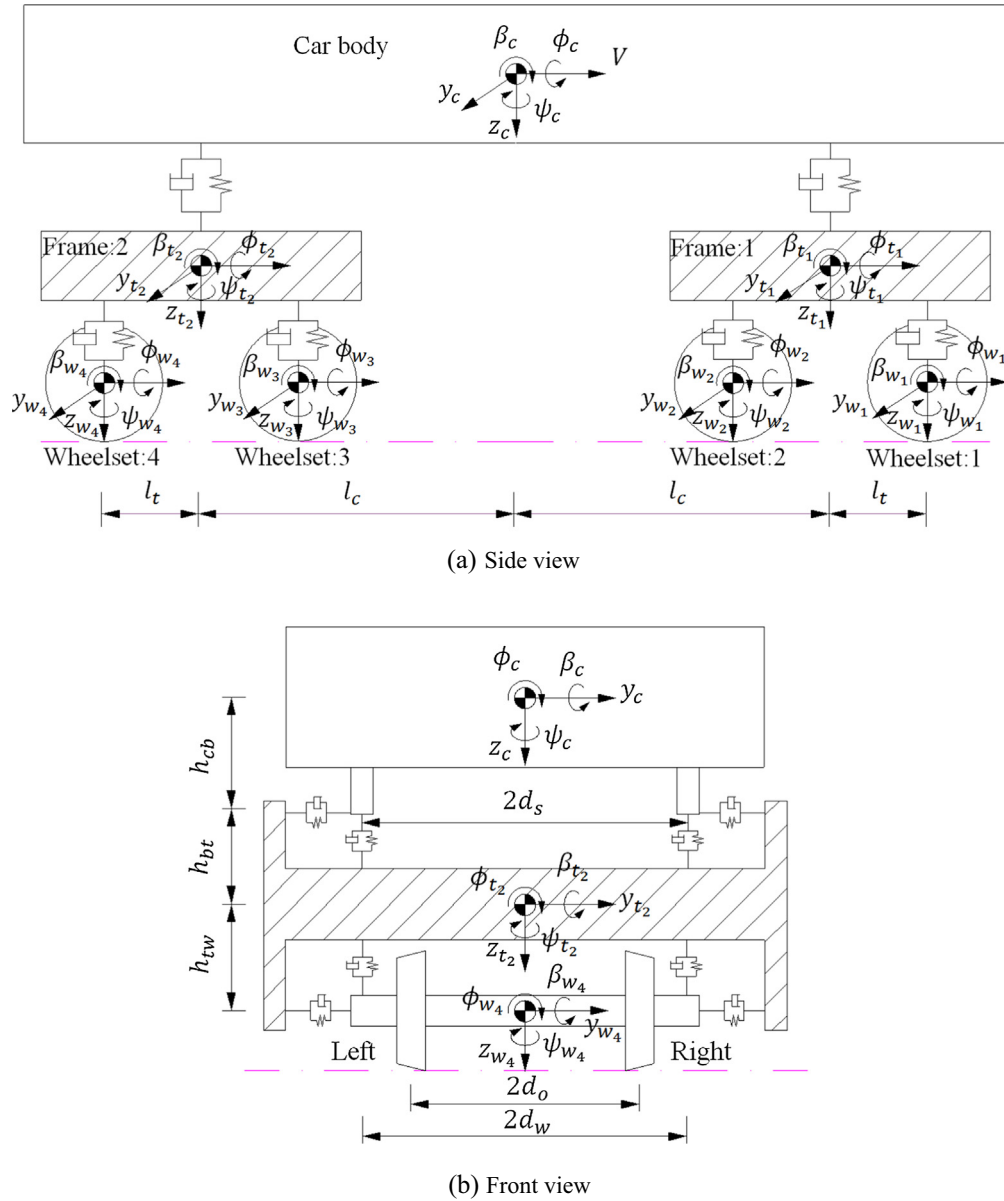


Fig. 1. Three dimensional dynamic model of the railway vehicle system.

$$\mathbf{K}_v = \begin{bmatrix}
 \mathbf{K}_{cc} & \mathbf{K}_{ct_1} & \mathbf{K}_{ct_2} & 0 & 0 & 0 & 0 \\
 \mathbf{K}_{t_1c} & \mathbf{K}_{t_1t_1} & 0 & \mathbf{K}_{t_1w_1} & \mathbf{K}_{t_1w_2} & 0 & 0 \\
 \mathbf{K}_{t_2c} & 0 & \mathbf{K}_{t_2t_2} & 0 & 0 & \mathbf{K}_{t_2w_3} & \mathbf{K}_{t_2w_4} \\
 0 & \mathbf{K}_{w_1t_1} & 0 & \mathbf{K}_{w_1w_1} & 0 & 0 & 0 \\
 0 & \mathbf{K}_{w_2t_1} & 0 & 0 & \mathbf{K}_{w_2w_2} & 0 & 0 \\
 0 & 0 & \mathbf{K}_{w_3t_2} & 0 & 0 & \mathbf{K}_{w_3w_3} & 0 \\
 0 & 0 & \mathbf{K}_{w_4t_2} & 0 & 0 & 0 & \mathbf{K}_{w_4w_4}
 \end{bmatrix} \quad (5)$$

$$\mathbf{C}_v = \begin{bmatrix}
 \mathbf{C}_{cc} & \mathbf{C}_{ct_1} & \mathbf{C}_{ct_2} & 0 & 0 & 0 & 0 \\
 \mathbf{C}_{t_1c} & \mathbf{C}_{t_1t_1} & 0 & \mathbf{C}_{t_1w_1} & \mathbf{C}_{t_1w_2} & 0 & 0 \\
 \mathbf{C}_{t_2c} & 0 & \mathbf{C}_{t_2t_2} & 0 & 0 & \mathbf{C}_{t_2w_3} & \mathbf{C}_{t_2w_4} \\
 0 & \mathbf{C}_{w_1t_1} & 0 & \mathbf{C}_{w_1w_1} & 0 & 0 & 0 \\
 0 & \mathbf{C}_{w_2t_1} & 0 & 0 & \mathbf{C}_{w_2w_2} & 0 & 0 \\
 0 & 0 & \mathbf{C}_{w_3t_2} & 0 & 0 & \mathbf{C}_{w_3w_3} & 0 \\
 0 & 0 & \mathbf{C}_{w_4t_2} & 0 & 0 & 0 & \mathbf{C}_{w_4w_4}
 \end{bmatrix} \quad (6)$$

The external force vector acting on the vehicle from the track \mathbf{F}_{vt} is written as

$$\mathbf{F}_{vt} = \left\{ \mathbf{F}_c^T, \mathbf{F}_{t_1}^T, \mathbf{F}_{t_2}^T, \mathbf{F}_{w_1}^T, \mathbf{F}_{w_2}^T, \mathbf{F}_{w_3}^T, \mathbf{F}_{w_4}^T \right\}^T \quad (7)$$

where

$$\mathbf{F}_c = \mathbf{F}_{t_1} = \mathbf{F}_{t_2} = 0 \quad (8)$$

are the sub-force vectors acting on the car body, the front and the rear frame, respectively. \mathbf{F}_{w_i} ($i = 1, 2, 3, 4$) is the sub-force vector acting on the i th wheelset and can be expressed as

$$\mathbf{F}_{w_i} = \left\{ \begin{array}{l}
 Q_i^L + Q_i^R \\
 P_i^L + P_i^R + (m_w + m_t/2 + m_c/4)g \\
 d_0(P_i^R - P_i^L) - r_i^L Q_i^L - r_i^R Q_i^R + M_{ix}^L + M_{ix}^R + I_{wy} \dot{\psi}_{w_i} \\
 r_i^L (F_{ix}^L + N_{ix}^L) + r_i^R (F_{ix}^R + N_{ix}^R) + \psi_{w_i} (r_i^R Q_i^R + r_i^L Q_i^L) + M_{iy}^L + M_{iy}^R \\
 d_0 (F_{ix}^L + N_{ix}^L - F_{ix}^R - N_{ix}^R) + d_0 \psi_{w_i} (Q_i^L - Q_i^R) + M_{iz}^L + M_{iz}^R + I_{wy} \dot{\phi}_{w_i} \dot{\psi}_{w_i}
 \end{array} \right\} \quad (i = 1, 2, 3, 4) \quad (9)$$

where superscripts L and R indicate the left and right wheels; subscripts x , y and z indicate the longitudinal, lateral and vertical directions respectively; subscript i stands for the wheelset number. Q_i^α and P_i^α are the forces acting on the left wheel ($\alpha = L$) or the right wheel ($\alpha = R$) of the i th wheelset from rails in the positive y and z directions

$$\begin{cases} Q_i^\alpha = F_{iy}^\alpha + N_{iy}^\alpha \\ P_i^\alpha = F_{iz}^\alpha + N_{iz}^\alpha \end{cases} \quad (\alpha = L, R) \quad (10)$$

N_{ix}^α , N_{iy}^α and N_{iz}^α are the normal force components acting on the wheels in the x , y and z directions; M_{ix}^α , M_{iy}^α and M_{iz}^α are the moments acting on the wheels about the x , y and z directions; r_i^α are the instant rolling radius of the wheels on the i th wheelset; I_{wy} is the pitch moment of inertia of the wheelset; m_w , m_t and m_c are the mass of the wheelset, frame and car body respectively; g is the gravity acceleration; d_0 is half of the lateral distance between wheel-rail contact points.

2.2. Equations of motion of track subsystem

The two-layer flexible track model is composed of two parallel rails, mounted on sleepers by means of elastic fasteners, as shown in Fig. 2. The first layer of the track consists of rails, represented by simply supported Euler beams with a finite length discretely supported on the fasteners. The vertical and lateral bending and torsional deformations of the rails are all taken into account. Each sleeper in the second layer of the track is regarded as a rigid body with three DOFs of lateral displacement, vertical displacement and roll. The connections between the rails and the sleepers (fasteners) and the connections between the sleepers and the subgrade are represented by a set of linear spring-damper elements in the lateral and vertical directions. The motion of the subgrade is neglected. The rail cant is $1/40$.

Detailed equations of motion of the rails and the sleepers can be found in Ref. [18]. With the motion about the static equilibrium position as the object of this study, combining the equations of the rails and the sleepers in generalised coordinates, the general equation of the track system can be expressed in matrix form

$$\mathbf{M}_t \ddot{\mathbf{X}}_t + \mathbf{C}_t \dot{\mathbf{X}}_t + \mathbf{K}_t \mathbf{X}_t = \mathbf{F}_{tv} \quad (11)$$

where \mathbf{X}_t , $\dot{\mathbf{X}}_t$ and $\ddot{\mathbf{X}}_t$ are the vectors of displacement, velocity and acceleration of the track subsystem respectively. The displacement vector \mathbf{X}_t can be written as

$$\mathbf{X}_t = \left\{ (\mathbf{q}_r^L)^T, (\mathbf{q}_r^R)^T, \mathbf{x}_s^T \right\}^T \quad (12)$$

in which

$$\begin{cases} \mathbf{q}_r^L = \left\{ q_{y1}^L, \dots, q_{yK}^L, q_{z1}^L, \dots, q_{zK}^L, q_{\phi 1}^L, \dots, q_{\phi K}^L \right\}^T \\ \mathbf{q}_r^R = \left\{ q_{y1}^R, \dots, q_{yK}^R, q_{z1}^R, \dots, q_{zK}^R, q_{\phi 1}^R, \dots, q_{\phi K}^R \right\}^T \\ \mathbf{x}_s = \left\{ y_{s1}, \dots, y_{sN_s}, z_{s1}, \dots, z_{sN_s}, \phi_{s1}, \dots, \phi_{sN_s} \right\}^T \end{cases} \quad (13)$$

where q_{yk}^α , q_{zk}^α and $q_{\phi k}^\alpha$ are the k th modal coordinates of the left rail ($\alpha = L$) or the right rail ($\alpha = R$) in lateral and vertical bending, and torsion directions, respectively; $k = 1 \sim K$, K is the number of modes considered for the rail beam; y_{sj} , z_{sj} and ϕ_{sj} are the lateral, vertical and roll angular displacements of the j th sleeper, respectively.

\mathbf{M}_t , \mathbf{K}_t , \mathbf{C}_t are the mass, stiffness and damping matrices of the track system respectively and can be expressed as

$$\mathbf{M}_t = \text{diag} \left[\mathbf{M}_r^L, \mathbf{M}_r^R, \mathbf{M}_s \right] \quad (14)$$

$$\mathbf{K}_t = \begin{bmatrix} \mathbf{K}_{rr}^L & 0 & \mathbf{K}_{rs}^L \\ 0 & \mathbf{K}_{rr}^R & \mathbf{K}_{rs}^R \\ \mathbf{K}_{sr}^L & \mathbf{K}_{sr}^R & \mathbf{K}_{ss} \end{bmatrix} \quad (15)$$

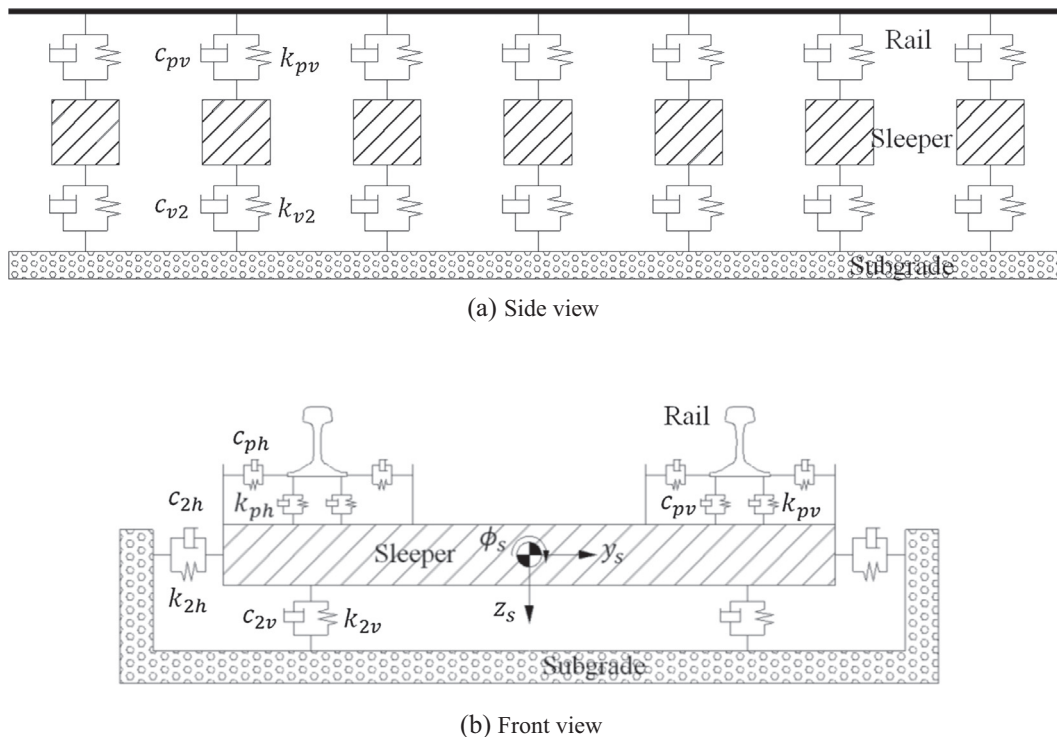


Fig. 2. Two-layer track system dynamic model.

$$C_t = \begin{bmatrix} C_{rr}^L & 0 & C_{rs}^L \\ 0 & C_{rr}^R & C_{rs}^R \\ C_{sr}^L & C_{sr}^R & C_{ss} \end{bmatrix} \quad (16)$$

The external force vector acting on the vehicle from the track F_{tv} is written as

$$F_{tv} = \{ (F_r^L)^T, (F_r^R)^T, F_s^T \}^T \quad (17)$$

where

$$\begin{cases} F_r^L = \left\{ -\sum_{i=1}^{N_w} Q_i^L Y_1(x_{w_i}), \dots, -\sum_{i=1}^{N_w} Q_i^L Y_K(x_{w_i}), -\sum_{i=1}^{N_w} P_i^L Z_1(x_{w_i}), \dots, \right. \\ \left. -\sum_{i=1}^{N_w} P_i^L Z_K(x_{w_i}), \sum_{i=1}^{N_w} M_{w_i}^L \Phi_1(x_{w_i}), \dots, \sum_{i=1}^{N_w} M_{w_i}^L \Phi_K(x_{w_i}) \right\}^T \\ F_r^R = \left\{ -\sum_{i=1}^{N_w} Q_i^R Y_1(x_{w_i}), \dots, -\sum_{i=1}^{N_w} Q_i^R Y_K(x_{w_i}), -\sum_{i=1}^{N_w} P_i^R Z_1(x_{w_i}), \dots, \right. \\ \left. -\sum_{i=1}^{N_w} P_i^R Z_K(x_{w_i}), \sum_{i=1}^{N_w} M_{w_i}^R \Phi_1(x_{w_i}), \dots, \sum_{i=1}^{N_w} M_{w_i}^R \Phi_K(x_{w_i}) \right\}^T \\ F_s = 0 \end{cases} \quad (18)$$

where N_w is the number of the wheelsets; x_{w_i} is the longitudinal coordinate of the i th wheelset; Y_k, Z_k and Φ_k are the k th mode shape functions of the lateral, vertical bending and torsion of the rail, respectively; $M_{w_i}^\alpha = -Q_i^\alpha h_r - P_i^\alpha e$ is the equivalent moment acting on the left rail ($\alpha = L$) or the right rail ($\alpha = R$) from the i th wheelset; h_r is the vertical distance from the rail's torsional center to the point of application of lateral wheel-rail force; e is the lateral distance from the rail's torsional center to the point of application of vertical wheel rail force.

2.3. Wheel-rail interaction model

The wheel-rail interaction model is the key component of the vehicle-track coupled system. It mainly includes three sub-models: the contact geometry model, the normal force model and the tangential creep force model. The wheel-rail contact geom-

etry model is used for describing the locations of the contact points on the wheel and rail interfaces and is the prerequisite for solving the wheel-rail forces. In traditional wheel-rail contact geometry computation method [19], the rails are assumed to be fixed without any movement and the wheel-rail contact geometry parameters are the nonlinear function of the lateral displacement and yaw angle of the wheelset. The wheelset rolling angle is adjusted iteratively until left and right minimum vertical distances between wheel and rail surfaces are equal. To consider the effect of the track vibration, especially the rail motions, the new wheel-rail contact geometry model [20] proposed by Chen and Zhai is used to solve the wheel-rail contact geometry relation. It considers the elastic deformation and instantaneous separation of the wheels and rails and avoids iterative solution of the wheelset rolling angle. To account for the instantaneous separation of the wheels from rails, the nonlinear Hertzian elastic contact theory is used to calculate the wheel-rail normal forces according to the elastic deformations of wheels and rails at contact points in the normal direction. In order to improve the accuracy of creep forces estimations, the tangential wheel-rail creep forces are calculated by FASTSIM algorithm [21] which was based on Kalker's simplified theory. The FASTSIM algorithm has been widely used in multiple commercial software, such as NUCARS, SIMPACK, and UM. To better illustrate the wheel-rail interaction model, the definitions of the wheelset and rail coordinates are shown in Fig. 3.

The detailed solution process of the wheel-rail contact geometry relation is described as follows:

Step 1: By solving the equations of motion of the vehicle and track subsystems, the instantaneous responses of the wheelset and the two rails at each time step are calculated.

Step 2: A line of points on the wheel profile where contact is possible, named contact locus, are obtained by the contact locus method [22]. Fig. 4 shows the contact geometry relation of the right wheel and right rail. C^R denotes the contact point of the right wheel and right rail.

For the known lateral displacement y_w , the known angle of attack ψ_w which refers to the yaw angle and the known roll angle ϕ_w of the wheelset, the contact locus on the tread of the right wheel can be determined by the following formulae

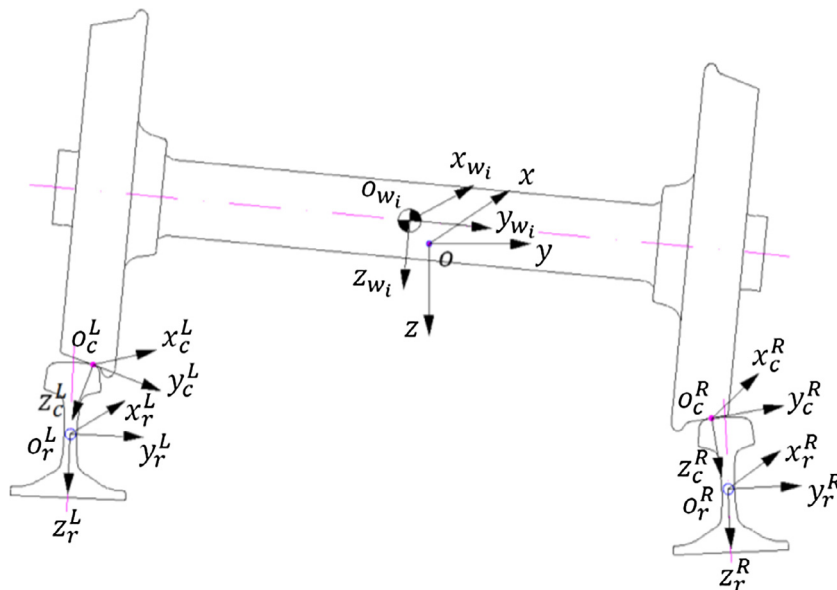


Fig. 3. Wheelset and rail coordinates.

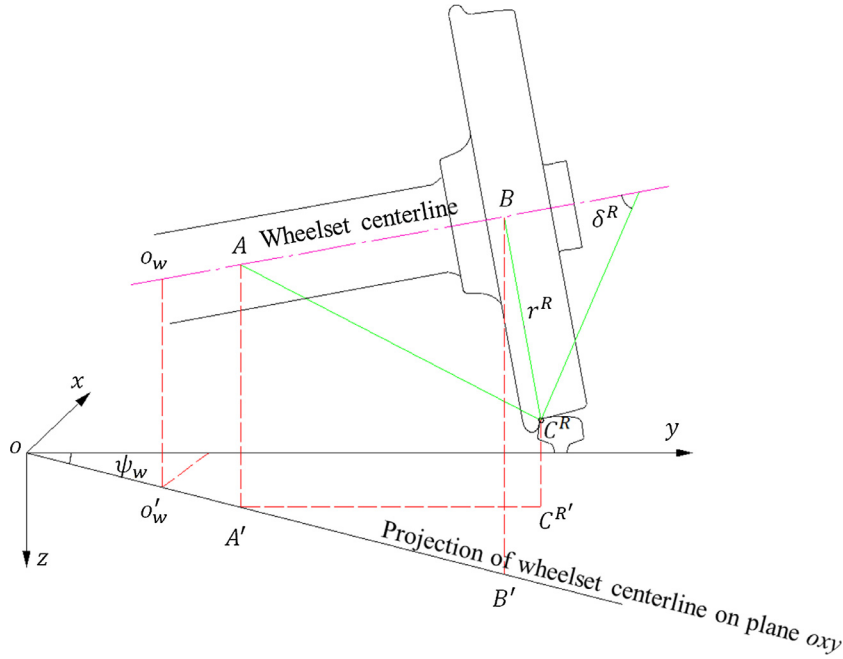


Fig. 4. The three-dimensional geometry relation between right wheel and right rail.

$$\begin{cases} x_c = b_w l_x + l_x r^R \tan \delta^R \\ y_c = b_w l_y - \frac{r^R}{1-l_x^2} (l_x^2 l_y \tan \delta^R + l_z m) + y_w \\ z_c = b_w l_z - \frac{r^R}{1-l_x^2} (l_x^2 l_z \tan \delta^R - l_y m) \end{cases} \quad (19)$$

where δ^R denotes the wheel-rail contact angle; r^R denotes the instant rolling radius of the wheels; b_w is the distance between the mass center of the wheelset and the contact point; the parameter $m = \sqrt{1 - l_x^2(1 + \tan^2 \delta^R)}$; l_x , l_y and l_z denote the direction cosines of the center line of the wheelset

$$\begin{cases} l_x = -\cos \phi_w \sin \psi_w \\ l_y = \cos \phi_w \cos \psi_w \\ l_z = \sin \phi_w \end{cases} \quad (20)$$

When b_w changes, a series of possible contact points form a curve called the “contact locus”. The contact locus for the left wheel-rail contact can be derived in the same way.

Step 3: The discretized rail dynamic profiles are calculated by transforming the reference frame in which the rail profile is defined to the absolute coordinate system, considering the rails displacements and irregularity.

Step 4: The wheel and rail profiles have been discretized and spline functions are then used to represent profiles so that the minimum vertical distance between the wheel and the rail for any position can be obtained by interpolation [23]

As shown in Fig. 5, the rail profile firstly projects on the contact locus to give the interpolated distances between wheel and rail and the minimum wheel-rail interpolation distance d_{\min} at the contact point is expressed in a discrete form

$$d_{\min} = \min(d_{z1}, d_{z2}, \dots, d_{zp}) \quad (21)$$

where $d_{zi} (i = 1, \dots, p)$ are the interpolated distance between the wheel and rail; p is the number of discrete points of the rail profile.

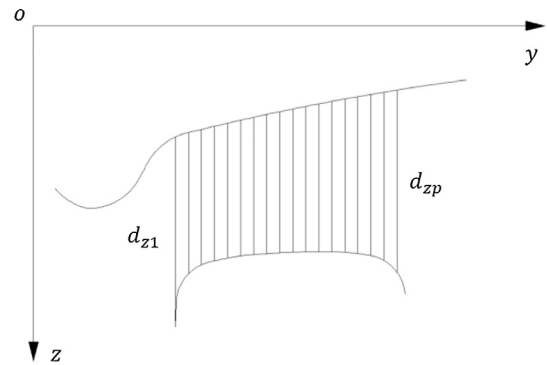


Fig. 5. The calculation method of the minimum vertical distance.

Step 5: The coordinates of contact points on the wheel and rail surfaces on both sides are obtained. Based on the known locations of the contact points, corresponding parameters at the contact points are acquired, such as instantaneous rolling radius of the wheels, contact angles, and curvature radius.

The wheel-rail normal force depends on the relative normal displacements between wheel and rail. Therefore, based on Hertzian nonlinear contact theory, it can be calculated as

$$N_{izc}^z(t) = \begin{cases} [\delta Z_{izc}^z / G]^{3/2} & \delta Z_{izc}^z > 0 \\ 0 & \delta Z_{izc}^z \leq 0 \end{cases} \quad (22)$$

where $G = 3.86 r_0^{0.115} \times 10^{-8}$ (m/N^{2/3}) is the wheel-rail contact constant [20], r_0 is the wheel’s nominal radius; δZ_{izc}^z is the normal displacements at the wheel rail contact points and $\delta Z_{izc}^z \leq 0$ means that the wheel lifts off from the rail. The normal displacements can be expressed as

$$\begin{cases} \delta Z_{izc}^L = (Z_{wi}(t) - (\Delta Z_{wi}^L(t) - \Delta Z_{wi}(0))) / \cos(\delta_i^L + \phi_{wi}) \\ \delta Z_{izc}^R = (Z_{wi}(t) - (\Delta Z_{wi}^R(t) - \Delta Z_{wi}(0))) / \cos(\delta_i^R - \phi_{wi}) \end{cases} \quad (23)$$

where $Z_{wi}(t)$ is the vertical displacement of the i th wheelset center of gravity at time t ; $\Delta Z_{wi}^z(t)$ is the minimum vertical distance

between the wheel and rail at time t , calculated by the wheel rail contact geometry model; $\Delta Z_{w_i}(0)$ is the minimum vertical distance at zero moment (due to symmetry relationship, $\Delta Z_{w_i}^L(0) = \Delta Z_{w_i}^R(0) = \Delta Z_{w_i}(0)$); δ_i^L, δ_i^R are the left and right wheel-rail contact angles, respectively.

Once the normal contact forces are known, the tangential creep forces and spin creep moment may be determined. The wheel-rail creep forces and spin creep moment are calculated by FASTSIM algorithm based on Kalker's simplified theory in this paper. The creep forces and the spin creep moment result from the tangential motion of the wheel relative to the rail in the contact region, therefore they depend on the creepages. Thus wheel-rail creepages should be calculated first. The longitudinal creepage $\zeta_{ix_c}^z$, lateral creepage $\zeta_{iy_c}^z$ and spin creepage $\zeta_{i\psi_c}^z$ can be defined as follows

$$\begin{cases} \zeta_{ix_c}^z = \Delta V_{ix_c}^z / V_i^z \\ \zeta_{iy_c}^z = \Delta V_{iy_c}^z / V_i^z \\ \zeta_{i\psi_c}^z = \Delta \omega_{iz_c}^z / \Delta \omega_{iz_c}^z \end{cases} \quad (24)$$

where $V_i^z = (V + r_i^z V \cos(\psi_{w_i}) / r_0) / 2$ is the real running speed of wheels; $\Delta V_{ix_c}^z, \Delta V_{iy_c}^z$ are the relative velocity components of the contact point in x_c^z and y_c^z axis of the wheel-rail contact coordinates, respectively; $\Delta \omega_{iz_c}^z$ is the relative angular velocity component about the z_c^z axis of the wheel-rail contact coordinates.

The relative velocity of the contact points on the wheel and rail interfaces in the wheel-rail contact coordinates are given below

$$\Delta \mathbf{V}_{ic}^z = \mathbf{T}_c^z \Delta \mathbf{V}_i^z \quad (25)$$

where \mathbf{T}_c^z is the transformation matrix from the absolute coordinate to the wheel-rail contact coordinates;

$\Delta \mathbf{V}_i^z = \{\Delta V_{ix}^z, \Delta V_{iy}^z, \Delta V_{iz}^z\}^T = \mathbf{V}_{w_i}^z - \mathbf{V}_r^z$ is the relative velocity of contact points in the absolute coordinate; $\mathbf{V}_{w_i}^z = \mathbf{V}_{ow_i} + \boldsymbol{\omega}_{w_i} \times \mathbf{R}_{w_i}^z$ is the absolute velocity of wheel at a contact point; \mathbf{V}_{ow_i} is the translational velocity of the center of mass of the i th wheelset in the absolute coordinate; $\boldsymbol{\omega}_{w_i}$ is the angular velocity of the i th wheelset in the absolute coordinate; $\mathbf{R}_{w_i}^z$ is the vector from the contact point to the center of mass of the wheelset; $\mathbf{V}_r^z = \{0, \dot{y}_r^z + \dot{j}_y^z, \dot{z}_r^z + \dot{j}_z^z\}^T$ is the absolute velocity of rail at the wheel-rail contact point; \dot{y}_r^z, \dot{z}_r^z are the lateral and vertical vibration velocities of rails, respectively; \dot{j}_y^z, \dot{j}_z^z are respectively lateral and vertical change rates of rail irregularities

$$\begin{cases} \dot{j}_y^z = \lim_{\Delta t \rightarrow 0} \frac{\Delta j_y^z(x)}{\Delta t} = V \cdot \lim_{\Delta x \rightarrow 0} \frac{\Delta j_y^z(x)}{\Delta x} = V \cdot \frac{\partial j_y^z(x)}{\partial x} \\ \dot{j}_z^z = \lim_{\Delta t \rightarrow 0} \frac{\Delta j_z^z(x)}{\Delta t} = V \cdot \lim_{\Delta x \rightarrow 0} \frac{\Delta j_z^z(x)}{\Delta x} = V \cdot \frac{\partial j_z^z(x)}{\partial x} \end{cases} \quad (26)$$

Similarly, the relative angular velocity between the wheelset and the rail in the wheel-rail contact coordinate

$\Delta \omega_{ic}^z = \{\Delta \omega_{ix_c}^z, \Delta \omega_{iy_c}^z, \Delta \omega_{iz_c}^z\}^T$ can be expressed as follows

$$\Delta \omega_{ic}^z = \mathbf{T}_c^z \Delta \omega_i^z \quad (27)$$

where $\Delta \omega_i^z = \{\Delta \omega_{ix}^z, \Delta \omega_{iy}^z, \Delta \omega_{iz}^z\}^T = \boldsymbol{\omega}_{w_i} - \boldsymbol{\omega}_r^z$ are the relative angular velocity between a wheelset and rail in the absolute coordinates;

$\boldsymbol{\omega}_r^z = \{\dot{\phi}_r^z, 0, 0\}^T$ is the absolute angular velocities of the rails.

So far, the longitudinal creepage $\zeta_{ix_c}^z$, lateral creepage $\zeta_{iy_c}^z$ and spin creepage $\zeta_{i\psi_c}^z$ of the i th wheelset at time t have been solved, and the wheel-rail creep forces $F_{x_c}^z, F_{y_c}^z$ and spin moment $M_{\psi_c}^z$ can be obtained by use of FASTSIM algorithm, together with the calcu-

lated normal forces $N_{iz_c}^z$ according to Eq. (22). The normal force and creep forces are all defined with respect to the wheel-rail contact coordinates. By coordinate transformations, creep forces and creep moment are obtained in the absolute coordinate. Finally the force vectors of the equations of motion of the vehicle and the track can be formed from Eqs. (7) and (17).

3. Iterative procedure based on prediction

A fast and accurate method for getting the wheel-rail forces at each time step is the key to determine the dynamic response of vehicle-track coupled system. The WLSE predictor is introduced to predict wheel-rail lateral force Q_i^z and vertical force P_i^z in the iteration process. Substituting the predicted forces into the equations of motion of the vehicle and the track respectively, dynamic response of each subsystem can be obtained. Then according to the response of wheelsets and rails and considering the track irregularity, the predicted forces are corrected by the wheel-rail interaction model. If the difference between the corrected and the predicted forces is greater than the specified tolerance, iteration continues until convergence is achieved. The relaxation technique is adopted to avoid the problem of numerical diffusion. The dynamic response of the vehicle-track coupled system can be determined efficiently by means of prediction of wheel-rail forces.

For convenience, taking $Q_{i,n}^{z,k}$ as an example, subscript $n \in [0, N_c]$ indicates the integration time $t_n = n\Delta t$, N_c is the total number of time steps, Δt is the time step; superscript k indicates the iteration number at time t_n , and $k = 0$ means the starting step of an iteration. The main solution procedure for the vehicle-track coupled dynamics consists of the following nine steps

Step 1: Inputting vehicle parameters and forming the mass matrix \mathbf{M}_v , stiffness matrix \mathbf{K}_v and damping matrix \mathbf{C}_v of the vehicle model according to Eqs. (4)–(6), respectively; Inputting track parameters and forming the mass matrix \mathbf{M}_t , stiffness matrix \mathbf{K}_t and damping matrix \mathbf{C}_t of the track model according to Eqs. (14)–(16), respectively;

Step 2: At time t_0 , setting the initial displacement, velocity and acceleration vectors of the vehicle and the track to zero: $\mathbf{X}_{v,0} = \mathbf{X}_{t,0} = \dot{\mathbf{X}}_{v,0} = \dot{\mathbf{X}}_{t,0} = \ddot{\mathbf{X}}_{v,0} = \ddot{\mathbf{X}}_{t,0} = 0$.

Step 3: At time t_1 , setting the starting value of iteration of wheel-rail vertical force: $P_{i,1}^{z,0} = -(m_w + m_t/2 + m_c/4)g$; Setting the starting value of iteration of wheel-rail lateral force and other forces to zero: $F_{ix,1}^{z,0} = N_{ix,1}^{z,0} = M_{ix,1}^{z,0} = M_{iy,1}^{z,0} = M_{iz,1}^{z,0} = M_{w_i,1}^{z,0} = 0$; Forming the starting value of iteration of the force vectors $\mathbf{F}_{vt,1}^0$ and $\mathbf{F}_{tv,1}^0$ by Eqs. (7) and (17), respectively.

Step 4: For $2 \leq n \leq N_c$, $F_{ix,n}^{z,0}, N_{ix,n}^{z,0}, M_{ix,n}^{z,0}, M_{iy,n}^{z,0}, M_{iz,n}^{z,0}$ and $M_{w_i,n}^{z,0}$ take the last converged value at time t_{n-1} ; In conventional iterative method, $Q_{i,n}^{z,0}$ and $P_{i,n}^{z,0}$ take the last converged value at time t_{n-1} . But in the present method, $Q_{i,n}^{z,0}$ and $P_{i,n}^{z,0}$ are predicted by the WLSE predictor (for the detailed algorithm see Section 4). Forming the starting value of iteration of the force vectors $\mathbf{F}_{vt,n}^0$ and $\mathbf{F}_{tv,n}^0$ by Eqs. (7) and (17), respectively.

Step 5: Calculating the starting value of iteration of the displacement, velocity and acceleration vectors of the vehicle $\mathbf{X}_{v,n}^0, \dot{\mathbf{X}}_{v,n}^0, \ddot{\mathbf{X}}_{v,n}^0$ and the track $\mathbf{X}_{t,n}^0, \dot{\mathbf{X}}_{t,n}^0, \ddot{\mathbf{X}}_{t,n}^0$ by substituting $\mathbf{F}_{vt,n}^0$ and $\mathbf{F}_{tv,n}^0$ into Eqs. (1) and (11), employing the explicit numerical integration method developed by Zhai [24].

$$\begin{cases} \mathbf{X}_{v,n}^0 = \mathbf{X}_{v,n-1} + \dot{\mathbf{X}}_{v,n-1}\Delta t + (1/2 + \gamma)\ddot{\mathbf{X}}_{v,n-1}\Delta t^2 - \gamma\ddot{\mathbf{X}}_{v,n-2}\Delta t^2 \\ \dot{\mathbf{X}}_{v,n}^0 = \dot{\mathbf{X}}_{v,n-1} + (1 + \varphi)\ddot{\mathbf{X}}_{v,n-1}\Delta t - \varphi\ddot{\mathbf{X}}_{v,n-2}\Delta t \\ \ddot{\mathbf{X}}_{v,n}^0 = \mathbf{M}_v^{-1}(\mathbf{F}_{vt,n}^0 - \mathbf{K}_v\mathbf{X}_{v,n-1} - \ddot{\mathbf{X}}_{v,n-1}((1 + \varphi)\mathbf{C}_v + (1/2 + \gamma)\mathbf{K}_v\Delta t)\Delta t \\ - \dot{\mathbf{X}}_{v,n-1}(\mathbf{C}_v + \mathbf{K}_v\Delta t) + \ddot{\mathbf{X}}_{v,n-2}(\varphi\mathbf{C}_v + \gamma\mathbf{K}_v\Delta t)\Delta t) \end{cases} \quad (28)$$

$$\begin{cases} \mathbf{X}_{t,n}^0 = \mathbf{X}_{t,n-1} + \dot{\mathbf{X}}_{t,n-1}\Delta t + (1/2 + \gamma)\ddot{\mathbf{X}}_{t,n-1}\Delta t^2 - \gamma\ddot{\mathbf{X}}_{t,n-2}\Delta t^2 \\ \dot{\mathbf{X}}_{t,n}^0 = \dot{\mathbf{X}}_{t,n-1} + (1 + \varphi)\ddot{\mathbf{X}}_{t,n-1}\Delta t - \varphi\ddot{\mathbf{X}}_{t,n-2}\Delta t \\ \ddot{\mathbf{X}}_{t,n}^0 = \mathbf{M}_t^{-1}(\mathbf{F}_{vt,n}^0 - \mathbf{K}_t\mathbf{X}_{t,n-1} - \ddot{\mathbf{X}}_{t,n-1}((1 + \varphi)\mathbf{C}_t + (1/2 + \gamma)\mathbf{K}_t\Delta t)\Delta t \\ - \dot{\mathbf{X}}_{t,n-1}(\mathbf{C}_t + \mathbf{K}_t\Delta t) + \ddot{\mathbf{X}}_{t,n-2}(\varphi\mathbf{C}_t + \gamma\mathbf{K}_t\Delta t)\Delta t) \end{cases} \quad (29)$$

in which, φ and γ are the integration parameters: $\varphi = \gamma = 0$ when $n = 1$ and $\varphi = \gamma = 1/2$ when $n \neq 1$. Based on the time-independent characteristics of vehicle and track system coefficient matrices, matrices $\mathbf{C}_v + \mathbf{K}_v\Delta t$, $(1 + \varphi)\mathbf{C}_v + (1/2 + \gamma)\mathbf{K}_v\Delta t$, \mathbf{M}_v^{-1} , $\varphi\mathbf{C}_v + \gamma\mathbf{K}_v\Delta t$, $\mathbf{C}_t + \mathbf{K}_t\Delta t$, $(1 + \varphi)\mathbf{C}_t + (1/2 + \gamma)\mathbf{K}_t\Delta t$, \mathbf{M}_t^{-1} and $\varphi\mathbf{C}_t + \gamma\mathbf{K}_t\Delta t$ only need to be calculated once and be called directly at each time step to reduce the computational cost.

Step 6: Calculating the corrected forces $Q_{i,n}^{z,1}$ and $P_{i,n}^{z,1}$ with the wheel-rail interaction model based on the calculated displacements and velocities of wheelsets and rails from step 5, considering the track irregularity. Forming the force vectors $\mathbf{F}_{vt,n}^1$ and $\mathbf{F}_{tv,n}^1$ by Eqs. (7) and (17), respectively. Calculating the relative error between the corrected forces $Q_{i,n}^{z,1}$, $P_{i,n}^{z,1}$ and the predicted forces $Q_{i,n}^{z,0}$, $P_{i,n}^{z,0}$ and then comparing the error with a specified tolerance as $\max(|(Q_{i,n}^{z,1} - Q_{i,n}^{z,0})/Q_{i,n}^{z,1}|) \leq \varepsilon$ and $\max(|(P_{i,n}^{z,1} - P_{i,n}^{z,0})/P_{i,n}^{z,1}|) \leq \varepsilon$, in which ε is the specified tolerance and its value is taken to be 1.0×10^{-5} in this study. If the convergence criterions are satisfied, return to Step 4 as the next time step; otherwise, go to Step 7 for the next iteration step.

Step 7: At time t_n , assuming that the k th iteration has been completed and the $(k + 1)$ th iteration is now being considered. Calculating forces $Q_{i,n}^{z,k+1}$ and $P_{i,n}^{z,k+1}$ with the wheel-rail interaction model based on the calculated displacements and velocities of wheelsets and rails at the k th iteration, considering the track irregularity. Introducing the relaxation method to improve forces $Q_{i,n}^{z,k+1}$ and $P_{i,n}^{z,k+1}$ by Eqs. (30) and (31) for the next iteration. Forming the force vectors $\mathbf{F}_{vt,n}^{k+1}$ and $\mathbf{F}_{tv,n}^{k+1}$ by Eqs. (7) and (17), respectively.

$$Q_{i,n}^{z,k+1} = Q_{i,n}^{z,k} + \eta(Q_{i,n}^{z,0} - Q_{i,n}^{z,k}) \quad (30)$$

$$P_{i,n}^{z,k+1} = P_{i,n}^{z,k} + \eta(P_{i,n}^{z,0} - P_{i,n}^{z,k}) \quad (31)$$

where η is the relaxation coefficient which has to be in a certain range ($0 < \eta < 1$) to ensure convergence. When the relaxation coefficient is within $0.2 < \eta < 0.4$, sufficient accuracy can be obtained with less computational time.

Step 8: Calculating the dynamic response of the vehicle and track at the $(k + 1)$ th iteration by substituting $\mathbf{F}_{vt,n}^{k+1}$ and $\mathbf{F}_{tv,n}^{k+1}$ into Eqs. (1) and (11). Calculating forces $Q_{i,n}^{z,k+2}$ and $P_{i,n}^{z,k+2}$ with the wheel-rail interaction model, considering the track irregularity. Step 9: Checking convergence of the solution. If $\max(|(Q_{i,n}^{z,k+2} - Q_{i,n}^{z,k+1})/Q_{i,n}^{z,k+2}|) \leq \varepsilon$ and $\max(|(P_{i,n}^{z,k+2} - P_{i,n}^{z,k+1})/P_{i,n}^{z,k+2}|) \leq \varepsilon$ are not satisfied, go to Step 7

and enter the next iteration step. Otherwise, output the results and go back to Step 4 for the next time step.

The iterative solution procedure above show that the present method based on prediction of wheel-rail forces only needs two layers of iteration loops and is easy to implement. Especially when Step 6 is executed, the iteration can be avoided and the computational efficiency can be enhanced significantly if the error between the predicted and the corrected forces satisfies the convergence criterion.

4. Weighted least squares error prediction method

The WLSE predictor has been successfully applied in many fields, such as navigation, industrial process control, and system identification, due to its adaptive and fast convergence nature [25]. In this paper, the WLSE predictor is introduced to predict wheel-rail forces.

The wheel-rail lateral force Q_i^z is taken as an example to illustrate the prediction procedure. According to the given M past forces $\bar{\mathbf{Q}}_n^z$ before time $t_n = n\Delta t$, the predicted force at time t_n can be expressed as

$$\hat{\mathbf{Q}}_{i,n}^z = \sum_{\vartheta=1}^M a_{n-\vartheta}^z \mathbf{Q}_{i,n-\vartheta}^z = (\mathbf{a}_n^z)^T \bar{\mathbf{Q}}_n^z \quad (32)$$

where M is the prediction order; $\mathbf{a}_n^z = \{a_{n-1}^z, a_{n-2}^z, \dots, a_{n-M}^z\}^T$ is the prediction coefficient vector, $a_{n-\vartheta}^z$ is the prediction coefficient; $\bar{\mathbf{Q}}_n^z = \{Q_{i,n-1}^z, Q_{i,n-2}^z, \dots, Q_{i,n-M}^z\}^T$.

The prediction error is defined as the difference between the predicted value $\hat{\mathbf{Q}}_{i,n}^z$ and the actual value $\mathbf{Q}_{i,n}^z$. In the WLSE algorithm, the weighted sum of the error is taken, and it will be minimized for a given set of weights. The coefficients should be changed adaptively to meet the minimum WLSE criterion as

$$\beta(\mathbf{a}^z) = \frac{1}{2} \sum_{\vartheta=1}^n \xi_{\vartheta} [(\mathbf{a}_{\vartheta}^z)^T \bar{\mathbf{Q}}_{\vartheta}^z - Q_{i,\vartheta}^z]^2 \quad (33)$$

where $\mathbf{a}^z = \{a_1^z, \dots, a_2^z, a_1^z\}^T$; $\bar{\mathbf{Q}}_{\vartheta}^z = \{Q_{i,\vartheta-1}^z, Q_{i,\vartheta-2}^z, \dots, Q_{i,\vartheta-M}^z\}^T$ is the given M past forces before time ϑ ; $\mathbf{a}_{\vartheta}^z = \{a_{\vartheta-1}^z, a_{\vartheta-2}^z, \dots, a_{\vartheta-M}^z\}^T$ is the prediction coefficient vector; $\hat{\mathbf{Q}}_{i,\vartheta}^z = (\mathbf{a}_{\vartheta}^z)^T \bar{\mathbf{Q}}_{\vartheta}^z$ is the predicted force; ξ_{ϑ} is the weight, here ξ_{ϑ} is set to be $\xi^{n-\vartheta}$ ($\vartheta = 1, 2, \dots, n$, $0 < \xi < 1$). Through weight ξ_{ϑ} , the older data points are increasingly less importance. Variable ξ is sometimes also referred to as the forgetting factor and usually $\xi = 0.99$ is used.

The WLSE predictor can be given as follows:

Step 1: Setting the predicted force at time t_1 : $\hat{\mathbf{Q}}_{i,1}^z = \mathbf{Q}_{i,1}^z$, where $\mathbf{Q}_{i,1}^z$ is calculated by the conventional iterative method.

Step 2: For $2 \leq n \leq N_c$, calculating the force $\hat{\mathbf{Q}}_{i,n}^z$ at time t_n

$$\hat{\mathbf{Q}}_{i,n}^z = (\mathbf{a}_n^z)^T \bar{\mathbf{Q}}_n^z \quad (34)$$

where $\mathbf{a}_2^z = \{1, 0, \dots, 0\}^T$; $\bar{\mathbf{Q}}_n^z = \{Q_{i,n-1}^z, Q_{i,n-2}^z, \dots, Q_{i,n-M}^z\}^T$, in which the forces with the subscript less than or equal to zero are set to zero.

Step 3: Updating the prediction coefficient vector as

$$\mathbf{a}_{n+1}^z = \mathbf{a}_n^z + \frac{\mathbf{B}_n^z \bar{\mathbf{Q}}_n^z}{\xi + (\bar{\mathbf{Q}}_n^z)^T \mathbf{B}_n^z \bar{\mathbf{Q}}_n^z} [Q_{i,n}^z - \hat{\mathbf{Q}}_{i,n}^z] \quad (35)$$

where $\mathbf{B}_2^z = \mathbf{I}$ (identity matrix of order M).

Step 4: Renewing matrix **B** as

$$\mathbf{B}_{n+1}^z = \frac{1}{\xi} \left\{ \mathbf{B}_n^z - \frac{\mathbf{B}_n^z \mathbf{Q}_n^z (\mathbf{Q}_n^z)^T \mathbf{B}_n^z}{\xi + (\mathbf{Q}_n^z)^T \mathbf{B}_n^z \mathbf{Q}_n^z} \right\} \quad (36)$$

Step 5: Returning to Step 2 for the next time step until the calculation is finished.

5. Numerical examples

A Chinese high speed train CRH2 vehicle model and a two-layer flexible track model are established in this study. The wheel-rail interaction model includes the effects of contact geometry and dynamic creep forces. Periodic cosine rail irregularity and measured rail irregularity are adopted in the simulation. Time step Δt is selected to be 0.01 ms. The main parameters of the vehicle system [26] and the track system [27] employed for analysis are listed in Tables 1 and 2, respectively. To validate the present method, the

Table 1
Main parameters of railway vehicle used for the analysis.

Parameter	Notation	Value	Unit
Car body mass	m_c	28,800	kg
Car body roll moment of inertia	I_{cx}	93,312	kg m ²
Car body pitch moment of inertia	I_{cy}	1,411,200	kg m ²
Car body yaw moment of inertia	I_{cz}	1331712	kg m ²
Frame mass	m_t	2600	kg
Frame roll moment of inertia	I_{tx}	2106	kg m ²
Frame pitch moment of inertia	I_{ty}	1424	kg m ²
Frame yaw moment of inertia	I_{tz}	2600	kg m ²
Wheelset mass	m_w	1728	kg
Wheelset roll moment of inertia	I_{wx}	740	kg m ²
Wheelset pitch moment of inertia	I_{wy}	115	kg m ²
Wheelset yaw moment of inertia	I_{wz}	740	kg m ²
Longitudinal stiffness of primary suspension per axle side	k_{px}	13,700	kN/m
Longitudinal damping of primary suspension per axle side	c_{px}	13.7	kN s/m
Lateral stiffness of primary suspension per axle side	k_{py}	5490	kN/m
Lateral damping of primary suspension per axle side	c_{py}	5.49	kN s/m
Vertical stiffness of primary suspension per axle side	k_{pz}	1244	kN/m
Vertical damping of secondary suspension per truck side	c_{pz}	19.6	kN s/m
Longitudinal stiffness of secondary suspension per bogie side	k_{sx}	159.7	kN/m
Longitudinal damping of secondary suspension per bogie side	c_{sx}	245	kN s/m
Lateral stiffness of secondary suspension per bogie side	k_{sy}	159.7	kN/m
Lateral damping of secondary suspension per bogie side	c_{sy}	58.8	kN s/m
Vertical stiffness of secondary suspension per bogie side	k_{sz}	990.8	kN/m
Vertical damping of secondary suspension per bogie side	c_{sz}	9.8	kN s/m
Half of longitudinal distance between bogie centers	l_c	8.75	m
Half of wheelbase	l_t	1.25	m
Nominal wheel radius	r_o	0.43	m
Half of the lateral distance between wheel-rail contact points	d_o	0.7465	m
Half of lateral distance between the primary suspensions of the two sides of the bogie	d_w	1.0	m
Half of lateral distance between the secondary suspensions of the two sides of the bogie	d_s	1.23	m
Vertical distance from frame center of gravity to wheelset center of gravity	h_{tw}	0.08	m
Vertical distance from frame center of gravity to secondary suspension	h_{bt}	0.49	m
Vertical distance from car body center of gravity to secondary suspension	h_{cb}	0.62	m

Table 2
Main parameters of two layer flexible track used for the analysis.

Parameter	Notation	Value	Unit
Rail mass per meter	m_r	60.64	kg/m
Sleeper mass	m_s	237.0	kg
Sleeper spacing	L_s	0.545	m
Elastic modulus of rail material	E_r	2.059×10^{11}	N/m ²
Rail moment of inertia about the horizontal axis	I_{ry}	3.22×10^{-5}	m ⁴
Rail moment of inertia about the vertical axis	I_{rz}	5.24×10^{-6}	m ⁴
Polar moment of inertia of rail section	I_{r0}	3.74×10^{-5}	m ⁴
Density of rail material	ρ_r	7.86×10^3	kg/m ³
Shear modulus of rail material	G_r	7.92×10^{10}	N/m ²
Torsional moment of inertia of rail section	I_{rt}	2.47×10^{-6}	m ⁴ /rad
Vertical distance from the center of twist to the point of application of lateral force	h_r	9.453×10^{-2}	m
Distance from the center of twist to the centroid of foot portion	a	8.147×10^{-2}	m
Half of lateral distance between two vertical forces from the fastening	b	7.5×10^{-2}	m
Half distance between the left and right rails	d	7.55×10^{-2}	m
Sleeper length	l_s	2.5	m
Rail cant		1/40	
Gauge		1.435	m
Poisson ratio of wheel and rail		0.3	
Wheel rail friction coefficient		0.35	
Lateral stiffness of rail fasteners	k_{ph}	1.47×10^4	kN/m
Lateral damping of rail fasteners	c_{ph}	26	kN s/rad
Vertical stiffness of rail fasteners	k_{pv}	7.8×10^4	kN/m
Vertical damping of rail fasteners	c_{pv}	50	kN s/rad
Lateral connection stiffness between sleepers and subgrade	k_{2h}	5.0×10^4	kN/m
Lateral connection damping between sleepers and subgrade	c_{2h}	40	kN s/rad
Vertical connection stiffness between sleepers and subgrade	k_{2v}	5.12×10^4	kN/m
Vertical connection damping between sleepers and subgrade	c_{2v}	20.298	kN s/rad

numerical results are compared with the commercial software NUCARS. The vehicle-track coupled dynamic model established in NUCARS is shown in Fig. 6. The efficiency is verified by comparison with the conventional iterative method. In addition, the predicted forces are compared with the last converged value at each time step to verify the accuracy of the WLSE predictor.

5.1. Periodic track irregularity

Periodic irregularity such as wheel out of roundness, dipped rail-joint, rail corrugation, are typical excitation sources existing in vehicle-track system. In this section, the dynamic response of a vehicle travelling at a constant speed of 100 km/h over the tangent track sections with periodic profile and alignment irregularities are calculated, respectively. The mathematical representations of the profile and alignment irregularities are the same and can be expressed as: $0.5A(1 - \cos 2\pi X/\lambda)$ [20], where peak-peak value $A = 10$ mm for the alignment irregularities and $A = -10$ mm for the profile irregularities, wave length $\lambda = 50$ m, X is track longitudinal distance. Figs. 7 and 8 display the track alignment and profile irregularities, respectively.

In order to avoid the effect of the irregularities in the initial segment, all the calculation results are selected after 50 m and the starting value of the longitudinal displacement is set to zero. Figs. 9–11 give time histories of the lateral displacements of the 1st wheelset, wheel-rail lateral forces of the 1R wheel which refers to the right wheel of the 1st wheelset, and lateral accelerations of

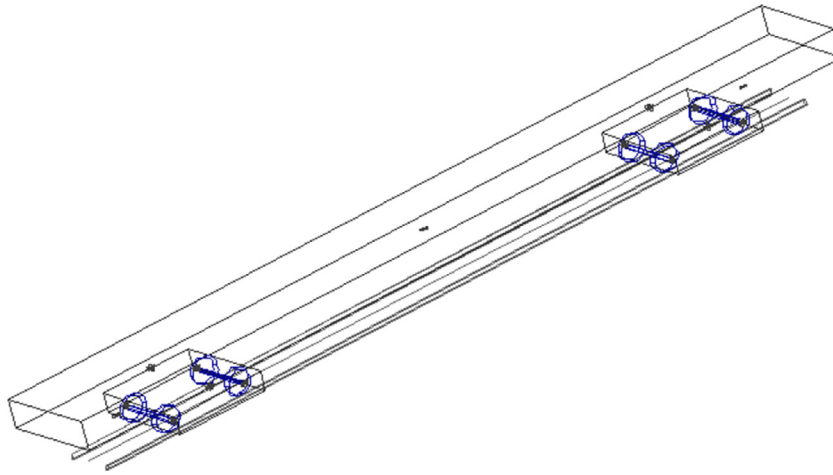


Fig. 6. Vehicle-track coupled dynamic model established in NUCARS.

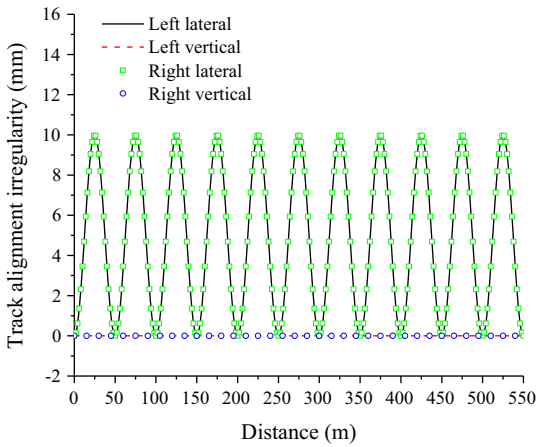


Fig. 7. Track alignment irregularity.

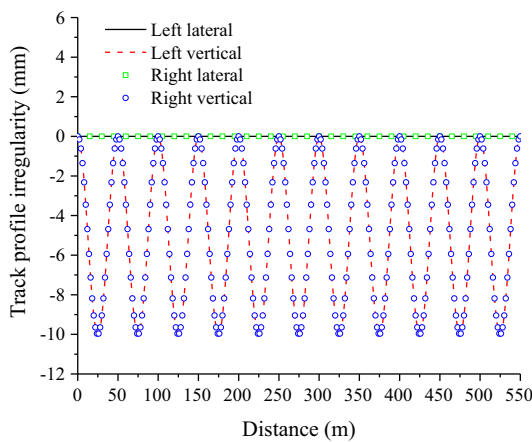


Fig. 8. Track profile irregularity.

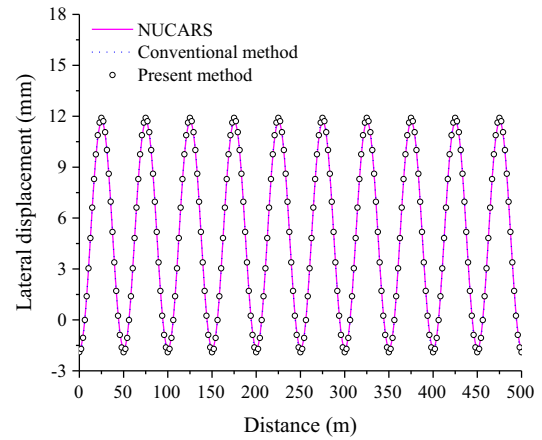


Fig. 9. Lateral displacement of the 1st wheelset with alignment irregularity.

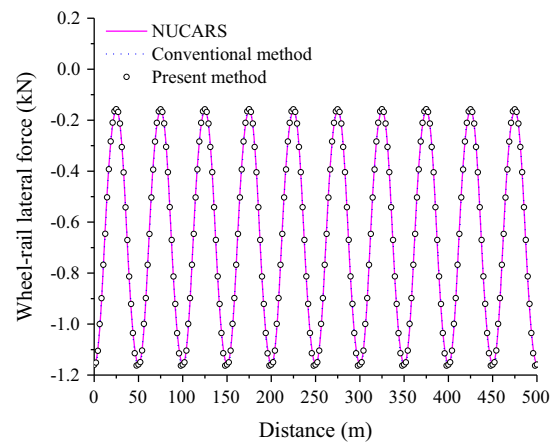


Fig. 10. Wheel-rail lateral force of the 1R wheel with alignment irregularity.

the center of mass of the car body respectively, under the excitation of track alignment irregularity, calculated by NUCARS, the conventional iterative method and the present method. As shown in Figs. 9–11, the results calculated by these three methods are quite consistent. Figs. 12–14 give time histories of the vertical displacements of the 1st wheelset, wheel-rail vertical forces of the 1R wheel, and vertical accelerations of the center of mass of the car

body, respectively, under the excitation of track profile irregularity, calculated by NUCARS, the conventional iterative method and the present method. It can be seen that the wheelset vertical displacement calculated by these three methods have little difference. The same is true for the car body vertical acceleration curves. The wheel-rail vertical forces calculated by the present method are larger than those obtained by NUCARS, but they have the same vari-

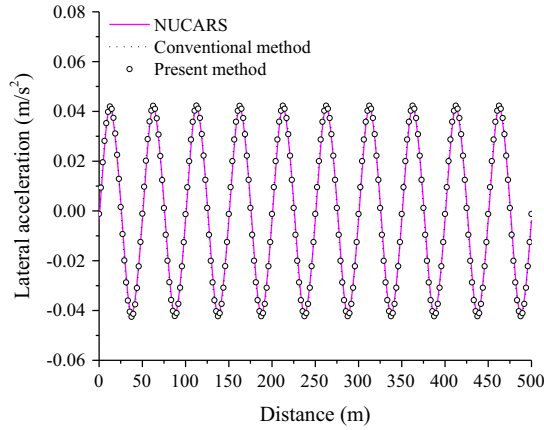


Fig. 11. Lateral acceleration of the center of mass of the car body with alignment irregularity.

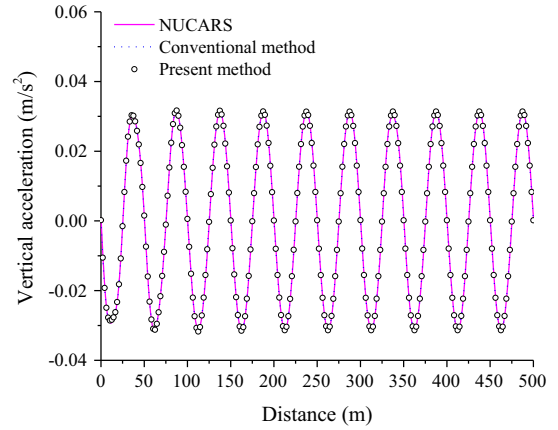


Fig. 14. Vertical acceleration of the center of mass of the car body with profile irregularity.

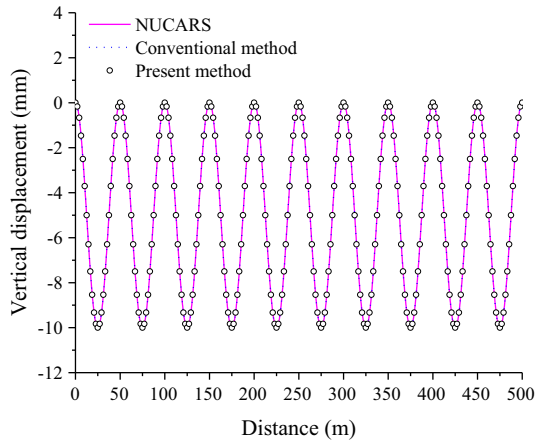


Fig. 12. Vertical displacement of the 1st wheelset with profile irregularity.

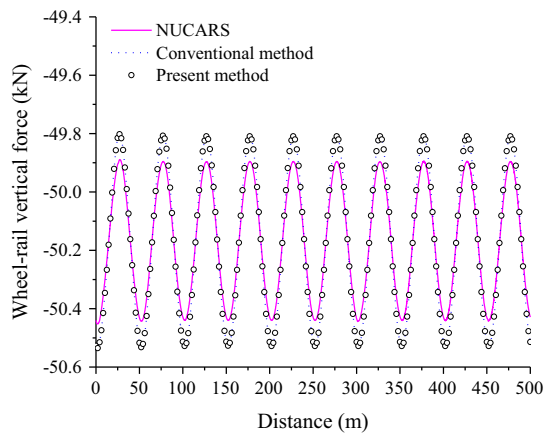


Fig. 13. Wheel-rail vertical force of the 1R wheel with profile irregularity.

ation tendency and the maximum relative error is 0.18% only. Through the results discussed above, the present method is verified to be reliable.

Due to the adoption of the same iterative strategy, the results calculated by the present method and conventional iterative method are almost identical. But the computational CPU time required for NUCARS, conventional iterative method and the pre-

Table 3
Statistical values of the number of iterations under alignment irregularity.

The number of iterations	Conventional method		Present method	
	Steps	Steps/total steps (%)	Steps	Steps/total steps (%)
2–4	83,574	3.07	37,111	1.97
5–9	50,362	1.85	14,693	0.78
10–19	17,150	0.63	4333	0.23
≥20	1361	0.05	245	0.013

Table 4
Statistical values of the number of iterations under profile irregularity.

The number of iterations	Conventional method		Present method	
	Steps	Steps/total steps (%)	Steps	Steps/total steps (%)
2–4	57,777	2.13	28,230	1.35
5–9	36,076	1.33	12,335	0.66
10–19	11,121	0.41	3177	0.17
≥20	813	0.03	150	0.008

sent method are 13.2 min, 25.3 min and 17.5 min respectively, under the excitation of track alignment irregularity. The efficiency of the present method is raised by 30.8% compared with the conventional iterative method but reduced by 32.5% compared with NUCARS. In the case of track profile irregularity excitation, the computational CPU time required for NUCARS, conventional iterative method and the present method is 12.7 min, 25.1 min and 17.3 min respectively. The efficiency of the present method is raised by 31.1% compared with the conventional iterative method but reduced by 36.2% compared with NUCARS. Tables 3 and 4 give the statistical values of the number of iterations under track alignment and profile irregularity, respectively. The computation speed of the NUCARS software is faster than the present method and we should try to optimize the numerical code to improve the calculation efficiency of the present method in the future.

Fig. 15 compares the predicted wheel-rail lateral force with the last converged value at each time step under the excitation of track alignment irregularity. Similar agreement can be observed in Fig. 16 for wheel-rail vertical force under the excitation of track profile irregularity. As shown in Figs. 15 and 16, the predicted and the last converged values have little difference under the excitation of track periodic irregularity. This will improve the efficiency with no iteration or fewer iterations.

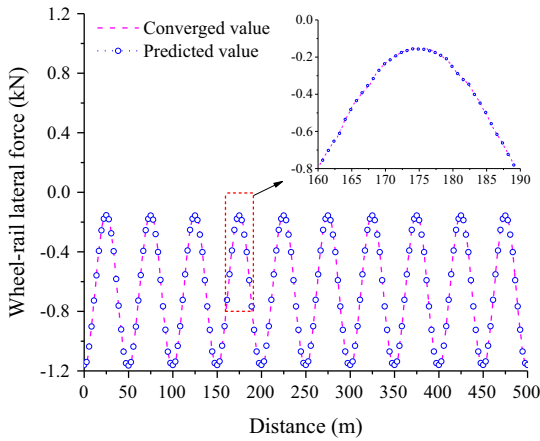


Fig. 15. Comparison of predicted and last converged values of wheel-rail lateral force with alignment irregularity.

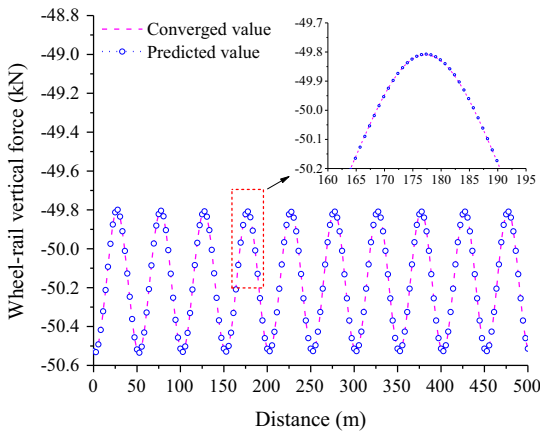


Fig. 16. Comparison of predicted and last converged values of wheel-rail vertical force with profile irregularity.

5.2. Measured track irregularity

One sample of measured track irregularity on Beijing-Tianjin Dedicated Passenger Line is used here as the system excitation, which is representative of real track irregularity. The vehicle speed is 200 km/h. Fig. 17 displays the vertical and lateral irregularities of

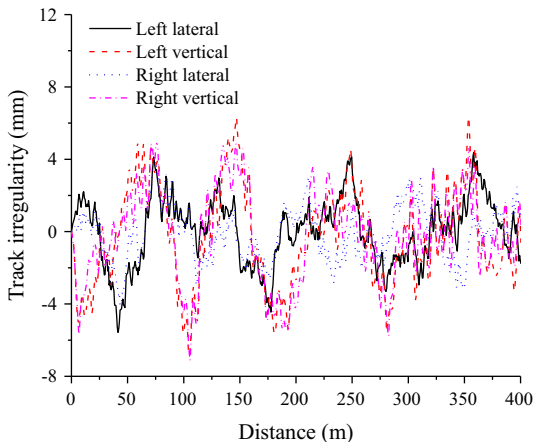


Fig. 17. Measured track irregularity.

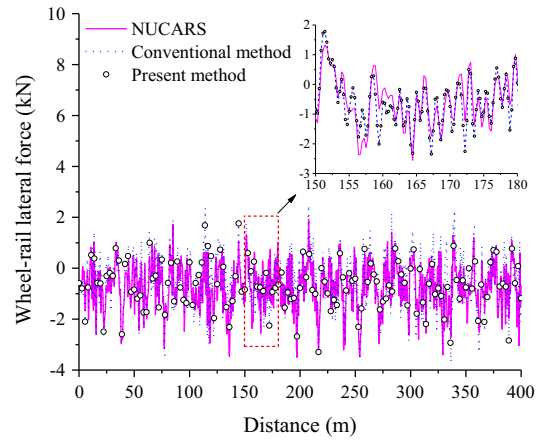


Fig. 18. Wheel-rail lateral force of the 1R wheel with measured irregularity.

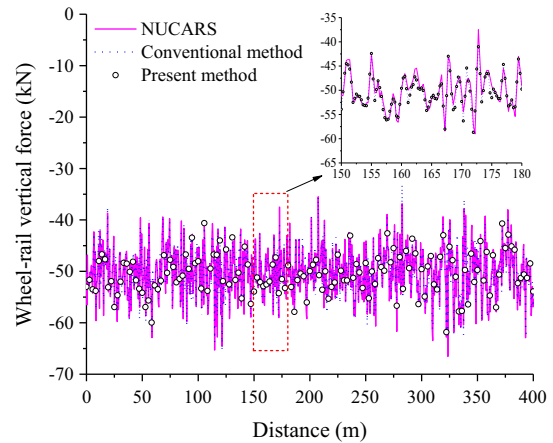


Fig. 19. Wheel-rail vertical force of the 1R wheel with measured irregularity.

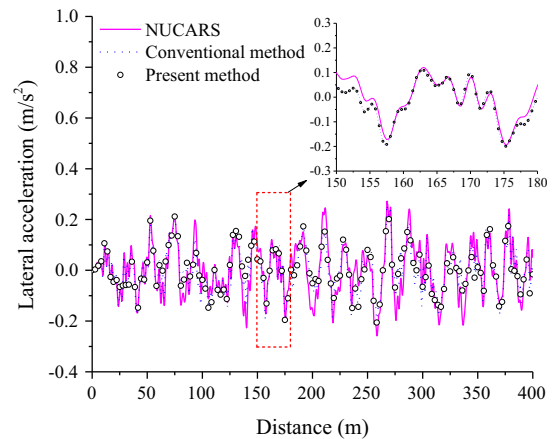


Fig. 20. Lateral acceleration of the center of mass of the car body with measured irregularity.

the left and right rails representing the Beijing-Tianjin Dedicated Passenger Line condition. Figs. 18–21 give time histories of the lateral and vertical forces of the 1R wheel, lateral and vertical accelerations of the center of mass of the car body, respectively, calculated by NUCARS, the conventional iterative method and the present method. The maximum absolute values are compared in Table 5. As can be seen in Figs. 18–21 and from Table 3, the results

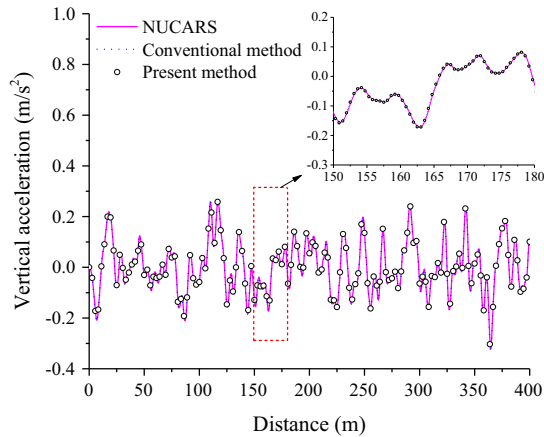


Fig. 21. Vertical acceleration of the center of mass of the car body with measured irregularity.

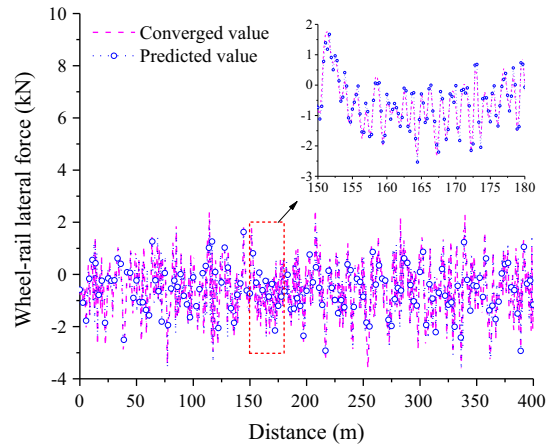


Fig. 22. Comparison of predicted and last converged value of wheel-rail lateral force with measured irregularity.

Table 5
Maximum absolute values of vehicle response.

Calculation method	Maximum absolute values of wheel-rail forces (kN)		Maximum absolute values of car body acceleration (m/s ²)	
	Lateral	Vertical	Lateral	Vertical
NUCARS	3.510	66.533	0.272	0.327
Conventional method	3.682	65.479	0.257	0.329
Present method	3.682	65.479	0.257	0.329

calculated by the conventional iterative method and the present method are almost identical. The trends of lateral dynamic response calculated by the present method are basically in good accordance with NUCARS. Compared with NUCARS, the relative error of the maximum absolute values of the wheel-rail lateral forces and car body lateral accelerations are 4.9% and 5.5%, respectively. The trends of the vertical dynamic response are more consistent with NUCARS than the lateral dynamic response. The relative error of maximum absolute values of the wheel-rail vertical forces and car body vertical accelerations are 1.58% and 0.6%, respectively. Through the numerical results discussed above, the accuracy of the present method is further verified.

Due to the adoption of the same iterative strategy, the results calculated by the present method and the conventional iterative method are almost identical. But the computational CPU time required for the NUCARS, conventional iterative method and the present method is 25.7 min, 45.6 min and 34.2 min respectively, under the measured track irregularity excitation. The computational efficiency of the present method is raised by 25% compared with the conventional method but reduced by 33.1% compared with NUCARS. Table 6 gives the statistical values of the number of iterations under measured track irregularity. Figs. 22 and 23 compare the predicted wheel-rail lateral and vertical forces with the last converged value at each time step respectively. The efficiency of the present method is further verified.

Table 6
Statistical values of the number of iterations under measured irregularity.

The number of iterations	Conventional method		Present method	
	Steps	Steps/total steps (%)	Steps	Steps/total steps (%)
2–4	365,058	7.45	191,071	5.19
5–9	115,642	2.36	72,894	1.98
10–19	79,381	1.62	41,969	1.14
≥20	40,671	0.83	20,985	0.57

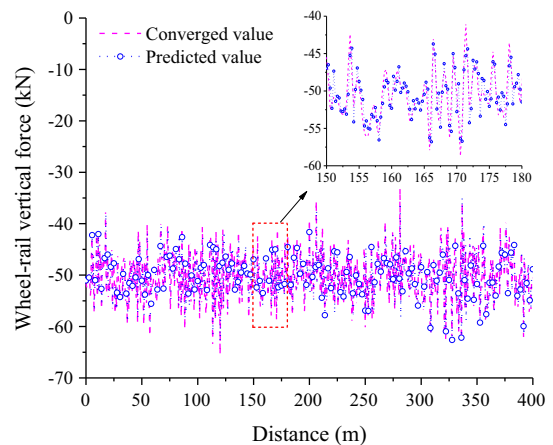


Fig. 23. Comparison of predicted and last converged value of wheel-rail vertical force with measured irregularity.

The main reasons for the differences are that the wheel-rail interaction model used in the present method is different from the one used in NUCARS, embodied in the following aspects: (1) the wheel-rail contact geometry model: the new wheel-rail contact geometry model proposed by Chen and Zhai [20] is used in the present method, while the method used in NUCARS is not described in enough detail in its Help file. (2) the solution method for wheel-rail normal forces: in the present method, nonlinear Hertzian contact theory is used while penetration contact model is used in NUCARS. In addition, the processing methods of the wheel rail profiles and track irregularity may also have some degrees of differences.

6. Conclusions

In this paper, an iterative method based on prediction of wheel rail forces is proposed and applied to determine the dynamic response of a vehicle-track coupled system. The Weighted Least-Squares Error (WLSE) predictor is introduced into the iterative solution process. By efficient prediction of wheel-rail forces and adoption of relaxation technique, the problems of difficult in convergence or the excessive number of iterations in the conventional iterative process can be avoided. The present method not only enhances the efficiency but also ensures the solution accuracy. The dynamic response of the vehicle to the excitation of periodic

and measured track irregularities is obtained by NUCARS, the conventional iterative method and the present method respectively in numerical examples. The accuracy of the present method and the vehicle-track coupled dynamic model especially the wheel-rail interaction model are validated by comparing the numerical results with NUCARS. The efficiency is verified by comparing the present method with the conventional iterative method. Numerical results show that the computational efficiency of the present method under excitation form the periodic and the measured track irregularities is raised by 30% and 25% respectively. The advantages of the present method will become more prominent as more effective predictors are introduced. In addition, practical wheel and rail profiles, detailed wheel-rail contact geometry relations and nonlinear wheel-rail creep forces are all considered in the wheel-rail interaction model. With the wheel-rail interaction model, the level of details of the vehicle-track coupled model is enhanced and the dynamic performance of a railway vehicle as related to safety and comfort can be evaluated more accurately.

Acknowledgments

The authors are grateful for support under grants from the National Science Foundation of China (11672060 and 11672052).

Appendix A. Notation

y, z	Lateral and vertical displacements in inertial coordinate system (m)	ϕ_{s_j}	sleeper (m)
ϕ, β, ψ	Roll, pitch and yaw angular displacements in inertial coordinate system (rad)	N_w	Roll angular displacements of the j th sleeper (rad)
V	Speed (km/h)	x_{w_i}	Number of wheelsets
t	Time (s)	Y_k, Z_k, Φ_k	Longitudinal coordinate of the i th wheelset (m)
L, R	Left and right side of the vehicle or track	$M_{w_i}^z$	k th mode shape functions of the lateral, vertical bending and torsion of the rail
α	$\alpha = L$ or $\alpha = R$	h_r	Equivalent moment acting on rails from the i th wheelset (N · m)
Q_i^L, Q_i^R	Forces acting on the left and right wheel of the i th wheelset from the track in the positive y direction (N)	e	Vertical distance from the rail torsional center to the point of application of lateral wheel-rail force (m)
P_i^L, P_i^R	Forces acting on the left and right wheel of the i th wheelset from the track in the positive z direction (N)	C^R	Lateral distance from the rail torsional center to the point of application of vertical wheel rail force (m)
$N_{ix}^z, N_{iy}^z, N_{iz}^z$	Normal force components acting on the i th wheelset in the x, y and z directions (N)	y_w	Contact point of the right wheel and right rail
$M_{ix}^z, M_{iy}^z, M_{iz}^z$	Moments acting on the i th wheelset about the x, y and z directions (N · m)	ψ_w	Wheelset lateral displacement (m)
r_i^z	Instant rolling radius of the wheels of the i th wheelset (m)	ϕ_w	Wheelset yaw angle (rad)
I_{w_y}	Pitch moment of inertia of the wheelset (kg · m ²)	δ	Wheelset roll angle (rad)
m_w	Wheelset mass (kg)	b_w	Wheel-rail contact angle (rad)
m_t	Frame mass (kg)	x_c, y_c, z_c	Distance between the wheelset centroid and the contact point (m)
m_c	Car body mass (kg)	l_x, l_y, l_z	Wheel rail contact point coordinates
g	Gravity acceleration (m/s ²)	d_{\min}	Direction cosines of the center line of the wheelset
d_0	Half of the lateral distance between wheel-rail contact points (m)	$d_{zi}(i = 1, \dots, p)$	Minimum wheel-rail interpolation distance
$q_{y_k}^L, q_{y_k}^R$	k th modal coordinates of the left and right rail in the y direction	p	Interpolated distance between the wheel and rail
$q_{z_k}^L, q_{z_k}^R$	k th modal coordinates of the left and right rail in the z direction	$N_{iz_c}^z$	Number of discrete points of the rail profile
q_{tk}^L, q_{tk}^R	k th modal coordinates of the left and right rail in the torsion direction	G	Wheel-rail normal force
K	Number of modes considered for the rail beam	r_0	Wheel-rail contact constant (m/N ^{2/3})
y_{s_j}, z_{s_j}	Lateral and vertical displacements of the j th	$\delta z_{iz_c}^z$	Nominal radius of the wheel (m)
		Z_{w_i}	Normal displacements at the wheel-rail contact points (m)
		$\Delta Z_{w_i}^z$	Vertical displacement of the i th wheelset centroid (m)
		δ_i^L, δ_i^R	Minimum vertical distance between the wheel and rail profiles (m)
		$\zeta_{ix_c}^z$	Left and right wheel-rail contact angles (rad)
		$\zeta_{iy_c}^z$	Longitudinal creepage
		$\zeta_{i\psi_c}^z$	Lateral creepage
		V_i^z	Spin creepage (1/m)
		x_c^z, y_c^z, z_c^z	Real running speed of wheels (m/s)
		$\Delta V_{ix_c}^z, \Delta V_{iy_c}^z$	Wheel-rail contact coordinates (m)
		$\Delta V_{ix}^z, \Delta V_{iy}^z$	Relative velocity components of the contact points in the x_c^z and y_c^z axis of the wheel-rail contact coordinates (m/s)
		ΔV_{iz}^z	Relative velocity of contact points in the absolute coordinate (m/s)
		$\Delta \omega_{iz_c}^z$	Relative angular velocity component about the z_c^z axis of the wheel-rail contact coordinates (rad/s)
		$\Delta \omega_{ix_c}^z, \Delta \omega_{iy_c}^z$	Relative angular velocity of the contact points in the absolute coordinate (rad/s)
		\dot{y}_r^z, \dot{z}_r^z	Lateral and vertical vibration velocities of rails (m/s)
		j_y^z, j_z^z	Lateral and vertical change rates of rail irregularities (m/s)
		$\dot{\phi}_r^z$	Absolute angular velocities of the rails (rad/s)
			Normal forces (N)

$N_{iz_c}^z$	
$F_{x_c}^z, F_{y_c}^z$	Wheel-rail creep forces (N)
$M_{\psi_c}^z$	Spin moment (N · m)
t_n	Simulation time (s)
n	Time step number
N_c	Total number of time steps
Δt	Time step (s)
φ, γ	Integration parameters
ε	Specified tolerance
η	Relaxation coefficient
M	Prediction order
$a_{n-\vartheta}^z$	Prediction coefficient
ξ_{ϑ}	Weight
ζ	Forgetting factor
A	Peak-peak value (mm)
λ	Wave length (m)
X	Track longitudinal distance (m)
$\mathbf{X}_v, \dot{\mathbf{X}}_v, \ddot{\mathbf{X}}_v$	Displacement, velocity and acceleration vectors of the vehicle
$\mathbf{M}_v, \mathbf{K}_v, \mathbf{C}_v$	Mass, stiffness and damping matrix of the vehicle
\mathbf{F}_{vt}	Force vector acting on the vehicle from the track
$\mathbf{X}_t, \dot{\mathbf{X}}_t, \ddot{\mathbf{X}}_t$	Displacement, velocity and acceleration vectors of the track
$\mathbf{M}_t, \mathbf{K}_t, \mathbf{C}_t$	Mass, stiffness and damping matrix of the track
\mathbf{F}_{tv}	Force vector acting on the track from the vehicle
$\mathbf{X}_{v,0}, \dot{\mathbf{X}}_{v,0}, \ddot{\mathbf{X}}_{v,0}$	Initial displacement, velocity and acceleration vectors of the vehicle
$\mathbf{X}_{t,0}, \dot{\mathbf{X}}_{t,0}, \ddot{\mathbf{X}}_{t,0}$	Initial displacement, velocity and acceleration vectors of the track
$\mathbf{X}_{v,n}^0, \dot{\mathbf{X}}_{v,n}^0, \ddot{\mathbf{X}}_{v,n}^0$	Starting value of iteration of the displacement, velocity and acceleration vectors of the vehicle at time t_n
$\mathbf{X}_{t,n}^0, \dot{\mathbf{X}}_{t,n}^0, \ddot{\mathbf{X}}_{t,n}^0$	Starting value of iteration of the displacement, velocity and acceleration vectors of the track at time t_n
$\mathbf{F}_{vt,n}^0, \mathbf{F}_{tv,n}^0$	Starting value of iteration of the force vectors
$\mathbf{F}_{vt,n}^k, \mathbf{F}_{tv,n}^k$	k th iteration value of iteration of the force vectors
$\Delta \mathbf{V}_{ic}^z$	Relative velocity vector at the contact points on the wheel and rail interfaces in the wheel-rail contact coordinates
\mathbf{T}_c^z	Transformation matrix from the absolute coordinate to the wheel-rail contact coordinates
$\Delta \mathbf{V}_i^z$	Relative velocity vector of contact points in the absolute coordinate
$\mathbf{R}_{w_i}^z$	Displacement vector from the contact point to the wheelset centroid
$\mathbf{V}_{o_{w_i}}$	Translational velocity vector of the center of mass of the i th wheelset in the absolute coordinate
$\boldsymbol{\omega}_{w_i}$	Angular velocity vector of the i th wheelset in the absolute coordinate
\mathbf{V}_r^z	Absolute velocity vector of the rail at the wheel-rail contact point
$\Delta \boldsymbol{\omega}_{ic}^z$	Relative angular velocity vector between the i th wheelset and the rail in the wheel-rail contact coordinate

$\Delta \boldsymbol{\omega}_i^z$	Relative angular velocity vector between the i th wheelset and rail in the absolute coordinates
$\boldsymbol{\omega}_r^z$	Absolute angular velocities vector of the rails
$\overline{\mathbf{Q}}_n^z$	Past forces vector
$\boldsymbol{\alpha}_n^z$	Prediction coefficient vector
\mathbf{I}	Identity matrix
\mathbf{B}	Renewing matrix

References

- [1] Knothe K, Grassie SL. Modelling of railway track and vehicle/track interaction at high frequencies. *Veh Syst Dynam* 1993;22(3–4):209–62.
- [2] Green MF, Cebon D. Dynamic response of highway bridges to heavy vehicle loads: theory and experimental validation. *J Sound Vib* 1994;170(1):51–78.
- [3] Green MF, Cebon D. Dynamic interaction between heavy vehicles and highway bridges. *Comput Struct* 1997;62(2):253–64.
- [4] Yang F, Fonder GA. An iterative solution method for dynamic response of bridge-vehicles systems. *Earthquake Eng Struct Dynam* 1996;25(2):195–215.
- [5] Xu YL, Zhang N, Xia H. Vibration of coupled train and cable-stayed bridge systems in cross winds. *Eng Struct* 2004;26(10):1389–406.
- [6] Majka M, Hartnett M. Effects of speed, load and damping on the dynamic response of railway bridges and vehicles. *Comput Struct* 2008;86(6):556–72.
- [7] Zhang N, Ge GH, Xia H, Li XZ. Dynamic analysis of coupled wind-train-bridge system considering tower shielding and triangular wind barriers. *Wind Struct* 2015;21(3):311–29.
- [8] Nguyen DV, Kim KD, Warnitchai P. Simulation procedure for vehicle-substructure dynamic interactions and wheel movements using linearized wheel-rail interfaces. *Finite Elem Anal Des* 2009;45(5):341–56.
- [9] Hawk H, Ghali A. Dynamic response of bridges to multiple truck loading. *Can J Civ Eng* 2011;8(3):392–401.
- [10] Marchesiello S, Fasana A, Garibaldi L, Piombo BAD. Dynamics of multi-span continuous straight bridges subject to multi-degrees of freedom moving vehicle excitation. *J Sound Vib* 1999;224(3):541–61.
- [11] Feriani A, Mulas M G, Candido L. Iterative procedures for the uncoupled analysis of vehicle-bridge dynamic interaction. In: *Proceedings of ISMA 2010 including USD2010, Katoomba*, 2010.
- [12] Vincenzi L, Savoia M, F Rossi. Vehicle-bridge interactive analyses on the lagoscuro viaduct. In: *Proceedings of the eleventh international conference on computational structures technology, Scotland*, 2012.
- [13] Lei XY, Wu SH, Zhang B. Dynamic analysis of the high speed train and slab track nonlinear coupling system with the cross iteration algorithm. *J Nonlinear Dynam* 2016:1–17.
- [14] Li Q, Xu YL, Wu DJ, Chen ZW. Computer-aided nonlinear vehicle-bridge interaction analysis. *J Vib Control* 2010;16(12):1791–816.
- [15] Li FS, Cheng D. The research on dynamic performance of 200 km/h CRH2 EMU vehicle. In: *Proceedings of 2011 international conference on electronic and mechanical engineering and information technology*; 2011, vol. 3, p. 1245–51.
- [16] Zhai WM, Wang KY, Cai CB. Fundamentals of vehicle-track coupled dynamics. *Veh Syst Dynam* 2009;47(11):1349–76.
- [17] Xiao XB, Jin XS, Deng YQ, Zhou ZR. Effect of curved track support failure on vehicle derailment. *Veh Syst Dynam* 2008;46(11):1029–59.
- [18] Xiao XB, Jin XS, Wen ZF. Effect of disabled fastening systems and ballast on vehicle derailment. *J Vib Acoust* 2007;129(2):217–29.
- [19] Garcia Vadiello E, Giménez JG, Tárrago JA. Wheel/rail contact: geometry study. *Veh Syst Dynam* 1984;13(4):207–14.
- [20] Chen G, Zhai WM. A new wheel/rail spatially dynamic coupling model and its verification. *Veh Syst Dynam* 2004;41(4):301–22.
- [21] Kalker J. A fast algorithm for the simplified theory of rolling contact. *Veh Syst Dynam* 1982;11(1):1–13.
- [22] Li ZL. Wheel-rail rolling contact and its application to wear simulation. PhD thesis. Delft University of Technology; 2002.
- [23] Ren ZS, Iwnicki SD, Xie G. A new method for determining wheel-rail multi-point contact. *Veh Syst Dynam* 2011;49(10):1533–51.
- [24] Zhai WM. Two simple fast integration methods for large-scale dynamics problems in engineering. *Int J Numer Meth Eng* 1996;39(24):4199–214.
- [25] Monzingo RA, Miller TW. *Introduction to adaptive arrays*. New York: John Wiley & Sons; 1980.
- [26] Zhang YG. Research on vibration behavior of CRH2-300 EMU trailer wheelset (in Chinese). Master Thesis. Beijing Jiaotong University; 2009.
- [27] Chen G. The analysis on random vibration of vehicle-track coupling system (in Chinese). PhD Thesis. Southwest Jiaotong University; 2000.